SIMULATION AND OPTIMIZATION OF A PNEUMATIC CONVEYING DEVICE FOR A PLOT WHEAT BREEDING HARVESTER BASED ON CFD–DEM

/

基于 CFD-DEM 的小麦小区育种收获机气力输送装置参数优化与试验

Liqing ZHAO[1*)], Xuechuan SHENG[1)], Guoying LI[2)], Cheng YANG[2)]
[1)] College of Mechanical and Electrical Engineering, Qingdao Agricultural University, Qingdao, 266109, China
[2)] Qingdao Plantech Mechanical Technology Co., Ltd, Qingdao, 266109, China
Tel: +86-13656390936; E-mail: zhlq017214@163.com
Corresponding author: Liqing Zhao
DOI: https://doi.org/10.35633/inmateh-78-121

Keywords: *Plot breeding harvester; CFD-DEM coupling; Pneumatic conveying; Residue rate*

ABSTRACT

To address the problem of grain residue commonly occurring during the operation of plot wheat breeding harvesters, the CFD–DEM coupling method was employed to investigate the airflow distribution characteristics and material conveying behavior within a pneumatic conveying device. Fan rotational speed, feeding rate, and the curvature radius of the lower conveying pipe were selected as experimental factors for single-factor and response surface experiments. The results showed that all selected factors significantly affected the conveying performance and residue rate. Specifically, the residue rate decreased with increasing fan rotational speed, increased with increasing feeding rate, and decreased as the curvature radius of the lower pipe increased. The response surface analysis indicated that the optimal operating parameters were a fan rotational speed of 2400 r/min, a feeding rate of 0.4 kg/s, and a lower pipe curvature radius of 420 mm, under which the minimum residue rate of 0.021% was achieved.

摘要

为解决小麦小区育种收获机在收获时易存在籽粒残留的问题，采用 CFD-DEM 耦合方法研究气力输送装置内气流分布特性及物料输送过程，选取风机转速、喂入量和下管道曲率半径为试验因素，开展单因素和响应面试验。试验结果表明，所选试验因素对试验结果均有显著影响，当风机转速增加时，残留率下降；当喂入量增加时，残留率上升；当下管道曲率半径增加时，残留率下降。响应面试验结果表明，当风机转速为 2400 r/min、喂入量为 0.4 kg/s、下管道曲率半径为 420 mm 时残留率最少，为 0.021％。

INTRODUCTION

As a key piece of equipment in field breeding trials, the plot breeding harvester directly affects the accuracy of breeding data through its operational precision and quality *(Wei et al., 2016; Dai et al., 2016; Zhu et al., 2015)*. Compared with conventional combine harvesters, the most critical performance indicator of a plot breeding harvester is the prevention of seed mixing. According to relevant industry standards, the residual rate after cleaning operations of a plot breeding harvester must be controlled at an extremely low level—typically less than 0.1%, and ideally approaching zero—to avoid cross-contamination of seeds between different experimental plots.

Pneumatic conveying technology is widely used in grain elevation in plot breeding harvesters due to its flexible layout and strong airflow self-cleaning capacity *(Li et al., 2023)*. However, during actual field operations, the material entering the pneumatic conveying device is not pure grain but inevitably contains short stalks and light impurities. There are significant differences in suspension velocity between wheat grains and short stalks; moreover, short stalks have a large aspect ratio, rough surfaces, and are prone to mechanical interlocking and bridging. When the mixed material flows through locations such as the feeder inlet of the device, it can easily induce airflow separation and secondary flow disturbances. This not only disrupts the stable gas-solid two-phase flow but also tends to cause material deposition inside the feeder, making it difficult for the residual rate of the device to meet the requirements of breeding operations. Therefore, the CFD-DEM coupling method is needed to analyze the movement of materials inside the pneumatic conveying device under the influence of airflow and to investigate the factors affecting the residual rate.

Liqing Zhao, Prof. Ph.D. Eng.; Xuechuan Sheng, M.S. Stud. Eng.; Guoying Li, Prof. Eng.; Cheng Yang, Sr. Eng.

In recent years, researchers worldwide have widely applied the CFD-DEM coupling method to optimize the parameters of agricultural equipment *(Hussain et al., 2025; Guzman et al., 2023; He et al., 2026; Liu et al., 2024; Li et al., 2025)*. *Yuan et al, (2023)* used this method to study the cleaning performance of flax threshing material in an air-and-screen cleaning device and analyzed the effects of louver screen opening angle, airflow velocity, vibration frequency, and amplitude on impurity rate and loss rate. *Li et al. (2025)* improved the auxiliary plate structure of a plot harvester through CFD-DEM coupled simulation, enhancing the Coanda effect to increase cleaning efficiency. *Bao et al. (2024)* systematically investigated the effects of corn particle density and diameter on trajectory deflection angle and explored the key factors affecting drag acceleration. *Kang et al. (2026)* studied the pneumatic conveying blockage of irregular corn cobs in a 90° vertical bend pipe and revealed the blockage mechanism in the downstream reacceleration zone. In summary, the CFD-DEM coupling method is conducive to research on the residual rate and working parameter optimization of the pneumatic conveying device in a wheat plot breeding harvester. *Wang et al. (2025)* used the CFD-DEM coupling method to study the effects of cell diameter, seed metering speed, number of cells per row, and negative pressure in the air chamber on the seed filling performance of the seed metering device.

Therefore, based on the CFD-DEM coupling method, this paper constructs a mixed-material simulation model containing wheat grains and short stalks, and analyzes the motion state of particles inside the pneumatic conveying device under the influence of airflow. Fan speed, feed rate, and *the lower pipe curvature radius* are selected as experimental factors, with the residual rate as the evaluation index. Single-factor and multi-factor experiments are conducted to analyze the effects of each factor and their interactions on material conveying. The optimal combination of parameters is then sought. This study aims to provide a theoretical basis and design reference for the subsequent development of low-residue plot breeding harvesting equipment.

MATERIALS AND METHODS

Establishment of the Simulation Model Structure

After the wheat plants are cut by the header, threshed by the threshing cylinder, and sieved by the louvered sieve, the material falls into the feeder. Under the airflow generated by the fan, pneumatic cleaning and pneumatic conveying take place, transporting the clean wheat grains to the grain tank. The pneumatic conveying device is shown in Fig.1.

The SOLIDWORKS software was used to establish a model of the pneumatic conveying device of the wheat plot breeding harvester. To accelerate the simulation computation speed, the established model was simplified by retaining its key working components, making it easier for simulation calculations without compromising the accuracy of the simulation test. The simplified model is shown in Fig.2. The length, width, and height of the pneumatic conveying device are 1230 mm, 265 mm, and 374 mm, respectively. The upper and lower curvature radii of the bend pipe at the front of the air inlet 1 are 600 mm and 520 mm, respectively, and the upper and lower curvature radii of the outlet bend pipe are 220 mm and 320 mm, respectively.

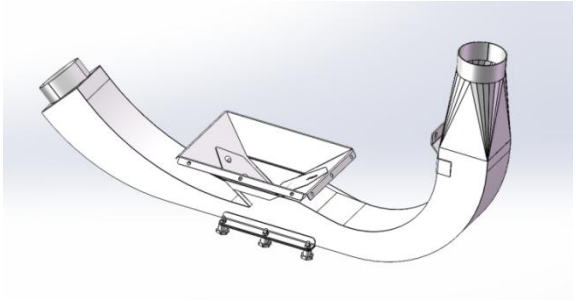

Fig. 1 - Pneumatic conveying device

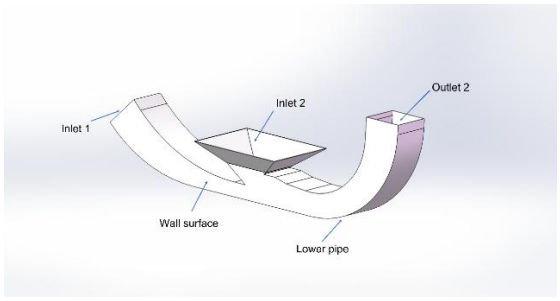

Fig. 2 - Simplified model of the pneumatic conveying device

Simulation of the mathematical model and the parameters settings

Establishment of the Wheat Threshing Material Discrete Element Model

A discrete element model of the threshed mixture from a wheat plot breeding harvester was established, requiring the physical property parameters of each component. The main components of the mixture were measured as wheat grains, short stalks, and light impurities, accounting for 90.28%, 4.22%, and 5.5% of the total mixture mass, respectively.

Since the light impurities are very light and easily discharged from the machine, only the effect of short stalks was considered in subsequent studies. The measured average length, width, and thickness of wheat grains were 6.43 mm, 3.08 mm, and 2.92 mm, respectively. The measured average length, outer diameter, and wall thickness of short stalks were 23.86 mm, 2.17 mm, and 0.37 mm, respectively. Based on the triaxial dimensions of wheat grains and short stalks, a multi-sphere particle filling method was used in EDEM software to establish the models. The resulting discrete element models of wheat grains and short stalks are shown in Fig.3.

Fig. 3 - Discrete element models of wheat grain and short stalk

Physical Properties and Contact Parameters of Wheat Threshing Material

Based on the conducted experiments and a review of the relevant literature, the Poisson's ratio (*Ning et al., 2019*), shear modulus, density, and, for each material interaction, the coefficient of restitution (Sun et al., 2025), static friction coefficient, and rolling friction coefficient (*Sun et al., 2025; Wang et al., 2021*) were determined. The shear modulus was obtained through compression tests using the TA.XTPlus texture analyzer from Stable Micro Systems, UK. The density was measured using an electronic balance and toluene solution by the liquid immersion method. Using an inclined plane friction tester, the static friction coefficients between different materials were measured by changing the materials of the test specimen and the inclined plane base plate. The attribute parameters of the discrete element model used in the simulation are shown in Table 1. The interaction parameters of each material are shown in Table 2.

Table 1

Material properties

Material	Poisson's ratio	Shear modulus (MPa)	Density/(kg/m³)
Grain	0.4	20	1350
Short stems	0.4	5	280
Wall surface	0.3	7800	7800

Table 2

The interaction parameters of each material

Contact form	Coefficient of restitution	Static Friction coefficient	Rolling friction coefficient
Grain-grain	0.42	0.45	0.01
Grain-short stem	0.25	0.55	0.01
Grain-wall surface	0.49	0.35	0.01
Short stem-short stem	0.28	0.38	0.01
Short stem-wall surface	0.68	0.32	0.01

Simulation of the mathematical model

Particle collision model

To ensure accurate simulation of collisions between particles and between particles and the screen surface, the Hertz-Mindlin (no-slip) contact model was adopted in EDEM software, and the particle motion was solved according to the mechanical equilibrium equations *(Dai et al., 2019; Guo et al., 2019)*.

$$m_P \frac{dv_P}{dt} = F_D + F_{GB} + F_{Sa} + F_{Ma} \quad (1)$$

$$I_P \frac{d\omega_P}{dt} = T \quad (2)$$

where:

m_P—the particle mass [kg];

v_p—the particle velocity [m/s];

t—the total simulation time [s];

F_D—the drag force [N];
F_{GB}—the gravitational force [N];
F_{Sa}—the Saffman lift force [N];
F_{Ma}—the Magnus lift force [N];
I_P—the particle moment of inertia [kg·m²];
ω_P—the particle angular velocity [rad/s];
T —the torque acting on the particle [N·m].

Fluid phase control model

During the coupling process, the gas phase is solved using the Navier-Stokes equations in Fluent software (*Xiao et al., 2018; Han et al., 2018*):

$$\frac{\partial \alpha_1 \rho}{\partial t} + \Delta \cdot \alpha_1 \rho u = 0 \quad (3)$$

where: ρ is the gas density (kg/m³); α_1 is the gas volume fraction; u is the airflow velocity (m/s).

Momentum conservation equation:

$$\Delta \cdot \alpha_1 \rho u^2 + \frac{\partial \alpha_1 \rho u}{\partial t} = -a_1 \Delta P + \alpha_1 \Delta \tau - S + \alpha_1 \rho g \quad (4)$$

$$S = \frac{\sum_{i=1}^{M} F_i}{V_{cell}} \quad (5)$$

where:

P is the pressure on the microelement [Pa]; g is the gravitational acceleration [m/s²]; S is the momentum source term; τ is the dynamic viscosity of the gas [Pa·s]; F_i is the drag force of particle i on the gas [N]; V_{cell} is the volume of the grid cell [m³].

Simulation of parameter settings

The fluid domain of the pneumatic conveying device was obtained by simplifying the model using Ansys Workbench Design Modeler. In the Meshing module, an unstructured tetrahedral mesh was used to mesh the pneumatic conveying device model, and mesh refinement was applied, as shown in Fig 4. After checking the mesh quality, the model was imported into Fluent software, with air selected as the fluid. The gravity direction was set to the negative Y-axis with a magnitude of 9.81 m/s². The standard κ-ε turbulence model was selected for calculation. Inlet1 was set as a velocity inlet with a velocity of 20 m/s, inlet 2 as a pressure inlet with a gauge pressure of 0, and outlet as a pressure outlet with a gauge pressure of 0. The simplified mesh model of the pneumatic conveying device was imported into EDEM software, and the Hertz–Mindlin no-slip contact model was selected. Particle models for wheat grains and short stalks were created and relevant parameters were input. A particle factory was set at inlet 2, and based on the mass ratio of wheat to short stalks, the wheat generation rate was set to 0.75 kg/s and the short stalk generation rate to 0.05 kg/s, with a particle generation time of 3 s. The gravity direction was set to the negative Y-axis with a magnitude of 9.81 m/s². The time step was set to 5×10^{-7} s, and the total simulation time was 4 s. The Fluent solver time step was set to 100 times the EDEM time step (*Wang et al., 2019*), 5×10^{-5} s, with 80,000 steps. After setting the coupling parameters, the simulation experiment was started.

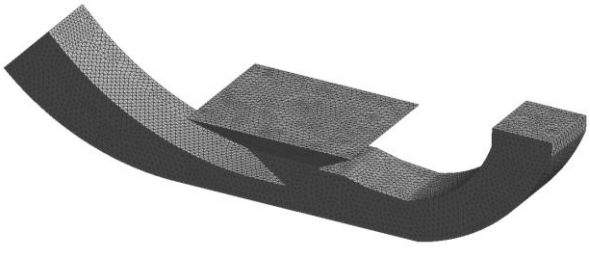

Fig. 4 - Mesh model

RESULTS

The convergence accuracy was set to 1×10^{-5}, and after the residual curves converged, the particle motion diagrams and airflow field distributions inside the device at different times were obtained. Fig.5 shows the particle motion diagrams at different times within the simulation time.

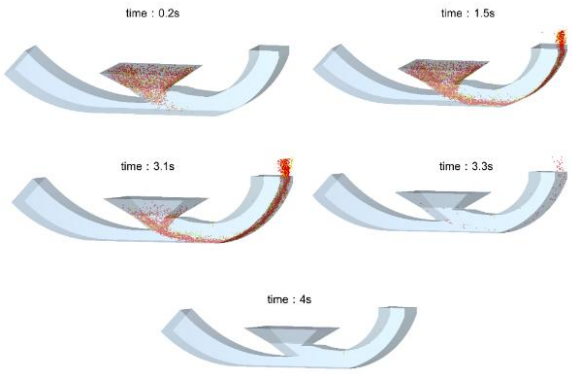

Fig. 5 - Simulation snapshots at different times

As shown in Figures 6 and 7, when the gas passes through the pipeline to the nozzle, the pipe diameter gradually decreases, causing the velocity to gradually increase. The velocity reaches its maximum at the nozzle, forming a stable jet flow. The interior of the feeder hopper appears dark blue, indicating that the airflow does not significantly enter the hopper but flows across the bottom of the hopper, and the material is not blown upward. This demonstrates the rationality of the designed feeder structure. Second, under the action of centrifugal force, the velocity on the outer side of the pipe is greater than that on the inner side, indicating that during conveying, the material accumulates toward the outer side of the bend pipe. Changing the lower pipe curvature radius directly affects the particle motion trajectory and the flow field variation.

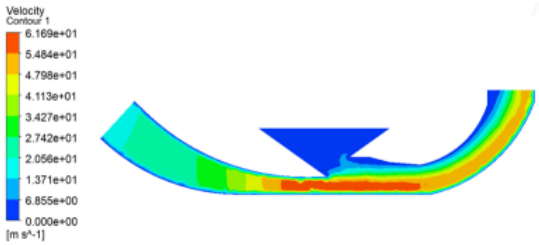

Fig. 6 - Velocity contour

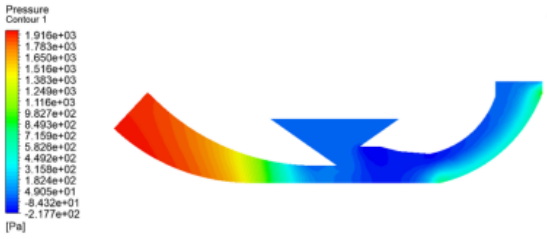

Fig. 7 - Static pressure

Single-factor simulation experiment

Fan speed, feed rate, and the lower pipe curvature radius were selected as experimental factors. The levels of each factor are shown in Table 3. The residual rate was selected as the experimental index. To quantitatively analyze the residual rate under the influence of different factors, a Total Mass Sensor was set outside the model in EDEM software to measure the total mass of remaining material in the simulation domain after the simulation ended. The calculation method is as follows:

$$\eta = \frac{m}{M} \times 100\,\% \qquad (6)$$

where:

η is the residual rate, [%]; m is the total mass of wheat grains and short stems remaining in the simulation domain at the end of the cleaning time, [kg]; M is the total mass of material cumulatively fed during the simulation process, [kg].

Table 3

Experimental factors and levels

Factor	Level				
Fan speed (r/min)	1800	2000	2200	2400	2600
Feeding rate (kg/s)	0.4	0.6	0.8	1.0	1.2
Lower pipe curvature radius (mm)	220	270	320	370	420

Influence of fan speed on residual rate

A single-factor simulation of fan speed was conducted with the feed rate controlled at 0.8 kg/s and the lower pipe curvature radius at 350 mm. The results are shown in the Fig 8. The residual rate gradually decreases with increasing fan speed.

When the fan speed is low, the air pressure generated by the fan is insufficient; the airflow velocity is just above the suspension velocity but cannot overcome the resistance of the bend pipe, causing material to deposit in the bend and at the bottom, resulting in a high residual rate. As the fan speed increases, the airflow carrying and purging capacities continuously improve, so the residual rate keeps decreasing and gradually approaches zero.

Influence of feeding rate on residual rate

In the single-factor simulation of feed rate, the fan speed was controlled at 2200 r/min and the lower pipe curvature radius at 350 mm. The effect of feed rate on the residual rate is shown in Fig 9. The residual rate increases continuously with increasing feed rate. When the feed rate is low, the conveying is in the dilute phase, with large particle spacing. The airflow generated by the fan can fully surround the material particles, resulting in a very low residual rate. As the feed rate increases, the spacing between particles decreases, gradually approaching dense phase conveying. The airflow penetration becomes insufficient, forming a tendency toward plug flow, leading to a sharp increase in the residual rate.

Influence of Lower Pipe Curvature Radius on residual rate

The effect of the lower pipe curvature radius on the residual rate was investigated with the fan speed controlled at 2200 r/min and the feed rate at 0.8 kg/s. As shown in Fig.10, the residual rate decreases continuously with increasing curvature radius of the lower pipe. When the lower pipe curvature radius is small, the conveying bend is sharp, resulting in a large system pressure drop. Particles directly impact the pipe wall in the acceleration section, causing significant kinetic energy loss, and thus the residual rate is high. As the lower pipe curvature radius gradually increases, the pipe becomes smoother, and particles can obtain sufficient vertical velocity component to pass through the elbow, so the residual rate keeps decreasing.

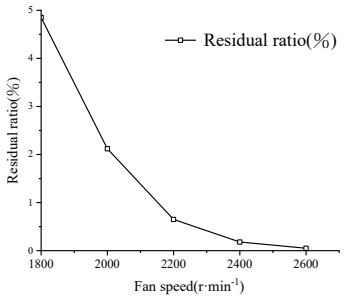

Fig. 8 - Effect of fan speed on residual rate

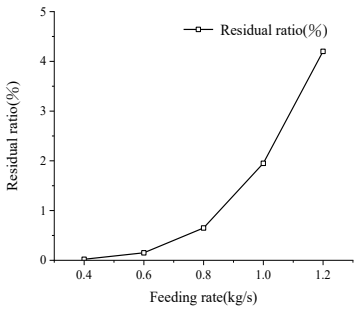

Fig. 9 - Effect of feeding rate on residual rate

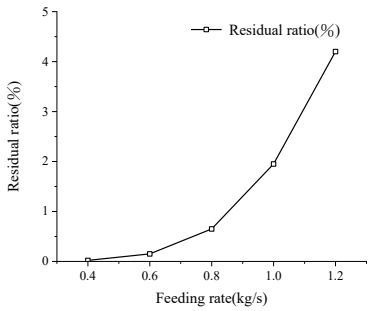

Fig 10 - Effect of lower pipe curvature radius on residual rate

Multi-factor simulation experiment

Test results and analysis of variance (ANOVA)

To determine the optimal parameter combination for the pneumatic conveying device, an experimental study was conducted on the effects of the interactions among fan speed, feed rate, and the lower pipe curvature radius on the residual rate of the device. According to the industry standard for plot breeding harvesters, the residual rate should be as low as possible; therefore, this experiment adopted 1% as the acceptance threshold for selecting experimental factors. The single-factor tests showed that the residual rate of the device was low when the fan speed was between 2200–2600 r/min, the feed rate between 0.4–0.8 kg/s, and the lower pipe curvature radius between 320–420 mm. Therefore, a response surface experiment was conducted with fan speed (A), feed rate (B), and the lower pipe curvature radius (C) as independent variables, and the wheat residual rate Y inside the pneumatic conveying device as the response index. The regression model was analyzed. The experimental factor levels are shown in Table 4, and the experimental results are shown in Table 5.

Table 4

The factor and level

Level	A (r/min)	B (kg/s)	C (mm)
-1	2200	0.4	320
0	2400	0.6	370
1	2600	0.8	420

Table 5

Response surface test results

Number	A (r/min)	B (kg/s)	C (mm)	Y (%)
1	2200	0.4	370	0.025
2	2600	0.4	370	0.028
3	2200	0.8	370	0.235
4	2600	0.8	370	0.155
5	2200	0.6	320	0.074
6	2600	0.6	320	0.075
7	2200	0.6	420	0.095
8	2600	0.6	420	0.065
9	2400	0.4	320	0.058
10	2400	0.8	320	0.105
11	2400	0.4	420	0.048
12	2400	0.8	420	0.065
13	2400	0.6	370	0.168
14	2400	0.6	370	0.015
15	2400	0.6	370	0.085
16	2400	0.6	370	0.062
17	2400	0.6	370	0.078

The Box-Behnken model in Design-Expert was used for experimental design and regression model analysis. The analysis of variance (ANOVA) results for the residual rate of the pneumatic conveying device are shown in Table 6.

As shown in Fig.6, the F-value of the established residual rate model is 53.45, with a corresponding p-value < 0.0001, indicating that the regression equation is highly significant and can well describe the relationship between the factors and the response value. The model fits well within the entire regression region and can be used for the prediction and analysis of the residual rate. The F-value for the lack-of-fit term is 2.11, with a p-value of 0.02421 < 0.05, indicating that the lack-of-fit is significant, suggesting a certain degree of lack-of-fit in the model. Considering that the overall F-value is high and highly significant, and the regression coefficient R^2 = 0.9857, indicating that the regression model explains 98.57% of the variation in the response value, and the adjusted coefficient R^2_{adj} = 0.9672, with the coefficient of determination and the adjusted coefficient being close to each other, indicating good accuracy and generality of the regression equation, the model still has high reference value.

Single-factor main effect analysis shows that fan speed (A), feed rate (B), and the lower pipe curvature radius (C) all have highly significant effects on the residual rate ($p < 0.001$). Based on the magnitude of the F-values, the order of the main effect intensity of each factor on the residual rate is: feed rate (B) > fan speed (A) > the lower pipe curvature radius (C).

Interaction effect analysis shows that the interaction term between fan speed and feed rate (AB) is highly significant, the interaction term between feed rate and the lower pipe curvature radius (BC) is significant, while the interaction term between fan speed and the lower pipe curvature radius (AC) is not significant.

Quadratic effect analysis shows that the quadratic term of fan speed (A^2) is highly significant, the quadratic term of feed rate (B^2) is significant, and the quadratic term of the lower pipe curvature radius (C^2) is not significant, indicating that the effects of fan speed (A) and feed rate (B) on the residual rate exhibit nonlinear characteristics, while the effect of the lower pipe curvature radius (C) is mainly linear.

The quadratic regression equation for the residual rate is obtained as follows:

$$Y=0.0674-0.0471x_1+0.0525x_2-0.0229x_3-0.0225x_1x_2+0.0032x_1x_3-0.0125x_2x_3 +0.0197x_1^2+0.0154x_2^2+0.0012x_3^2 \quad (7)$$

Table 6

ANOVA of simulation test results

Source	Sum of squares	df	F	P
Model	0.0495	9	53.45	＜0.0001
A	0.0178	1	172.62	＜0.0001
B	0.0221	1	214.24	＜0.0001
C	0.0042	1	40.67	0.0004
AB	0.0020	1	19.68	0.0030
AC	0.0000	1	0.4105	0.5421

Source	Sum of squares	df	F	P
BC	0.0006	1	6.07	0.0432
A^2	0.0016	1	15.84	0.0053
B^2	0.0010	1	9.73	0.0168
C^2	5.813E-06	1	0.0565	0.8190
Residual	0.0007	77		
Lack of fit	0.0004	3	2.11	0.02421
Pure error	0.0003	4		

Note: $P<0.05$ means significant，$P<0.01$ means extremely significant，$P>0.1$ means not significant.

Interaction analysis

As shown in Fig 11, fan speed and feed rate have an extremely significant interaction effect on the residual rate of the pneumatic conveying device. When the fan speed is at a low level and the feed rate is at a high level, the residual rate reaches its maximum value. As the feed rate increases, the residual rate increases significantly, while increasing the fan speed can effectively reduce the residual rate. This is because increasing the fan speed raises the airflow velocity and kinetic energy, enhances the material conveying capacity, and reduces the risk of accumulation caused by excessive feed rate.

The interaction between fan speed and the lower pipe curvature radius is not significant. The surface shown in Fig 12 is relatively smooth, indicating that the effects of these two factors on the residual rate are relatively independent. This means that increasing the lower pipe curvature radius can consistently reduce the residual rate at any fan speed. Similarly, the optimization effect of changing the lower pipe curvature radius on the residual rate is not significantly interfered by the current fan speed level. The effects of fan speed and the lower pipe curvature radius on the residual rate are relatively independent, and the coupling effect is weak.

As shown in Fig. 13, the interaction between feed rate and the lower pipe curvature radius is significant. When the feed rate is at a high level and the lower pipe curvature radius is at a low level, the residual rate reaches its maximum value. As the feed rate increases, the residual rate shows a clear increasing trend. As the curvature radius increases, the residual rate first decreases and then levels off. The interaction indicates that under high feed rate conditions, appropriately increasing the lower pipe curvature radius helps alleviate local material blockage, optimizes material flow passage, and thus reduces the residual rate.

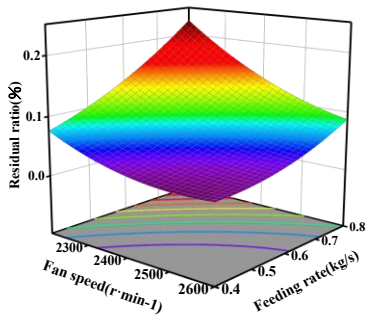

Fig. 11 - Interaction between fan speed and feed rate

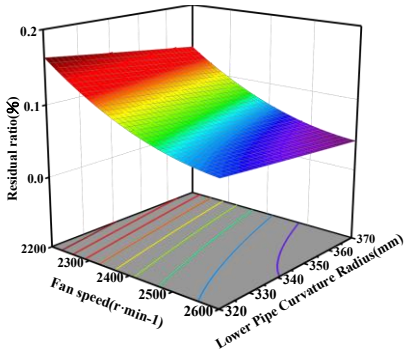

Fig. 12 - Interaction between fan speed and lower pipe curvature radius

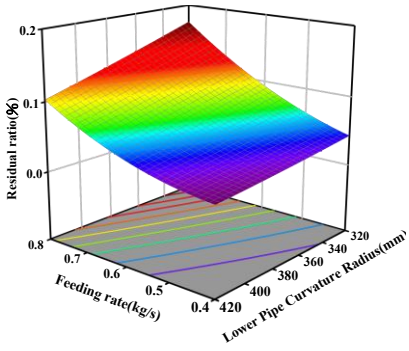

Fig. 13 - Interaction between feeding rate and lower pipe curvature radius

Parameter optimization and validation experiment

Parameter optimization

To improve the seed cleaning performance and harvesting efficiency of the plot breeding harvester, it is necessary to reduce the residual rate of the wheat harvester. Using the multi-objective optimization solving function in Design-Expert 13, with the objective of minimizing the residual rate, an optimization design was carried out for fan speed, feed rate, and curvature radius of the lower pipe. The three factor targets were set within the optimization ranges, and a parametric mathematical model was established as follows:

$$\begin{cases} \min Y \\ s.t. \begin{cases} 2200r/min \le A \le 2600r/min \\ 0.4kg/s \le B \le 0.8kg/s \\ 320mm \le C \le 420mm \end{cases} \end{cases}$$

After analysis, the coded levels of the three factors were obtained as 0, –1, and 1, respectively, i.e., fan speed of 2400 r/min, feed rate of 0.4 kg/s, and the lower pipe curvature radius of 420 mm. Substituting the coded values back into the regression equation, the wheat residual rate of the pneumatic conveying device was 0.021%.

Validation experiment

To verify the accuracy of the model prediction, three repeated experiments were conducted under the optimal parameter conditions. The average experimental value was 0.002176, and the relative error from the theoretical predicted value was 3.61%, which is less than 5%. The results indicate that the optimized parameter combination can effectively reduce the residual rate of the device, providing a theoretical basis for the structural design and operating parameter optimization of the pneumatic conveying device in the wheat plot harvester.

CONCLUSIONS

(1) A simulation model of the pneumatic conveying device of the wheat plot breeding harvester and a discrete element model of the materials were established. Through CFD-DEM coupled simulation, the movement of wheat grains and short stalks under the influence of airflow inside the device was obtained.

(2) Through single-factor experiments, the optimal experimental parameter intervals for each factor that meet the residual rate requirements of the wheat plot breeding harvester were determined: fan speed of 2200–2600 r/min, feed rate of 0.4–0.8 kg/s, and the lower pipe curvature radius of 320–420 mm.

(3) The optimal parameter combination obtained after multi-factor experimental parameter optimization was: fan speed of 2400 r/min, feed rate of 0.4 kg/s, and the lower pipe curvature radius of 420 mm, under which the residual rate of the pneumatic conveying device reached its minimum value of 0.021%. Validation experiments confirmed that this optimal parameter combination can effectively reduce the residual rate, providing research direction and theoretical support for the development of low-residue wheat plot harvesters.

ACKNOWLEDGEMENT

This research was funded by the National Key Research and Development Program (2023YFD2000404-1), and the Shandong Modern Agricultural Industry System Wheat Industry Innovation Team (SDAIT-01-13).

REFERENCES

[1] Bao, G.C., Zhang, Z.D., Yang, X.W., Liu, L.J., Li, J.D., Lu, Z.Y., Yang, W. (2024). Design and Experiment of Separating Impurities Device for Corn Plot Test Harvester Based on Coanda Effect (基于康达效应的玉米小区收获机除杂装置设计与试验) [J]. *Transactions of the Chinese Society for Agricultural Machinery*, Vol.55, No.10, pp. 234-243. Beijing/China.

[2] Dai, F., Zhao, W.Y., Han, Z.S., Li, X.K., Gao, A.M., Liu, X.L. (2016). Improvement and Experiment on 4GX-100 Type Wheat Harvester for Breeding Plots (4GX-100 型小区小麦种子收获机改进设计与试验) [J]. *Transactions of the Chinese Society for Agricultural Machinery*, Vol.47, No. S0, pp. 196-202. Beijing/China.

[3] Dai, F., Song, X.F., Zhao, W.Y., Han, Z.S., Zhang, F.W., Zhang, S.L. (2019). Motion simulation and test on threshed grains in tapered threshing and transmission device for plot wheat breeding based on CFD-DEM [J]. *International Journal of Agricultural and Biological Engineering*, Vol.12, No.01, pp. 66-73. Beijing/China.

[4] Guzman, L., Chen, Y., Landry, H. (2023). Coupled CFD-DEM Simulation of Seed Flow in Horizontal-Vertical Tube Transition [J]. *Processes*, Vol.11, pp. 909, Switzerland.

[5] Guo, B.J., Ma, X.D., Zhao, L., Yu, H.C., Ding, H.H., Dang, H. (2019). Mechanism Research on Separation of Paddy-Stalks Based on Discrete Element Method (基于离散单元法的稻米-茎秆分离机理研究) [J]. *Journal of Shenyang Agricultural University*, Vol.50, No.02, pp. 180-187. Shenyang/China.

[6] He, B., Zeng, H., Ge, Y., Li, G., Ma, C., Zheng, Y., Guo, Y. (2026). Optimization of structural parameters for the pneumatic conveying device of dried safflower filaments based on CFD-DEM coupling [J]. *Results in Engineering*, Vol.29, pp. 109092, Netherlands.

[7] Hussain, S., Chen, Y., Yu, X., Farid, M.U., Ghafoor, A., Alshamali, S.J., Munir, T., Hu, J. (2025). Design Optimization and Aerodynamic Investigations of Air Suction Seed Metering Systems through CFD-DEM Approach [J]. *Smart Agricultural Technology*, Vol.12, pp. 101082. Netherlands.

[8] Han, D.D., Zhang, D.X., Jing, H.R., Yang, L., Cui, T., Ding, Y.Q., Wang, Z.D., Wang, Y.X., Zhang, T.L. (2018). DEM-CFD coupling simulation and optimization of an inside-filling air-blowing maize precision seed-metering device [J]. *Computers and Electronics in Agriculture*, Vol.150, pp. 426-438, Netherlands.

[9] Kang, Y., Song, X., Luo, R., Huang, T., Xiao, F., Deng, Z., Chen, H. (2026). CFD-DEM simulation and parameter optimization of pneumatic conveying of threshed corn residual products in a vertical elbow [J]. *Industrial Crops and Products*, Vol.123, Elsevier, Amsterdam/Netherlands, pp. 123012. ISSN 0926-6690.

[10] Li, J.W., Yuan, W.S., Zhai, H.L., Zhu, S.S. (2023). Application of pneumatic conveying in agricultural machinery (气力输送技术在农业机械中的应用) [J]. *Journal of Chinese Agricultural Mechanization*, Vol.44, No.1, pp. 85-92,115. Nanjing/China.

[11] Liu, R., Zhang, G., Xiao, Y., Yan, B., Meng, Z., Dong, J., Wu, G. (2024). DEM-CFD investigation of particle motion characteristic in a guidance restraint-airflow blowing seed guiding device [J]. *Advanced Powder Technology*, Vol.35, pp. 104751, Netherlands.

[12] Li, H., Yang, L., Zhang, D., Tao, C., He, X., Xie, C., Li, C., Du, Z., Xiao, T., Li, Z., Wang, H. (2025). Design and optimization of a high-speed maize seed guiding device based on DEM-CFD coupling method [J]. *Computers and Electronics in Agriculture*, Vol.228, pp. 109999, Netherlands.

[13] Li, G.Y., Xu, Z.X., Li, G.L., Li, X., Lu, Z.H., Yu, R.Z., Yang, C. (2025). Design and Mechanism Study of Auxiliary Plate of New High-efficiency Impurity Removal Device for Plot Harvester Based on Coanda Effect (基于柯恩达效应的小区收获机高效除杂装置辅助板设计与机理研究) [J]. *Transactions of the Chinese Society for Agricultural Machinery*, Vol.56, No.12, pp. 343-353. Beijing/China.

[14] Ning, X.J., Jin, C.Q., Liu, P., Li, Q.L., Chen, Y.P. (2019). Research on screening performance of double layer vibrating screen for soybean harvester based on discrete element method [J]. American Journal of Agricultural Research, Vol.4, No.68, pp. 1-17. Houston/USA.

[15] Sun, K., Yu, J.Q., Zhao, J.W., Sun, Y.C., Yu, Y.J., Liang, L.S., Wang, Y. (2025). Parameter Calibration and Experimental Validation of Wheat Straw Model for Cutting Process Simulation (面向切割过程仿真的小麦茎秆模型参数标定与试验验证) [J]. *Transactions of the Chinese Society for Agricultural Machinery*, Vol.56, No.07, pp. 116-127. Beijing/China.

[16] Wang, W.W., Song, L.Z., An, X., Quan, L.Z., Xie, D.B., Chen, Y.X., Li, Z.D., Wu, Z.C., Chen, L.Q. (2025). Optimizing seed filling performance of the double-filling air suction maize and soybean seed metering device based on DEM-CFD coupling method [J]. *Computers and Electronics in Agriculture*, Vol.237, pp. 110586, Netherlands.

[17] Wang, W.Z., Liu, W.R., Yuan, L.H., Qu, Z., Zhang, H.M., Zhou, Z. (2021). Calibration of discrete element parameters of wheat plants at harvest period based on EDEM (基于 EDEM 的收获期小麦植株离散元参数标定) [J]. *Journal of Henan Agricultural University*, Vol.55, No.01, pp. 64-72. Zhengzhou/China.

[18] Wang, L.J., Feng, X., Zheng, Z.H., Yu, Y.T., Liu, T.H., Ma, Y. (2019). Design and Test of Combined Sieve of Maize Screening (玉米清选组合孔筛体设计与试验) [J]. *Transactions of the Chinese Society for Agricultural Machinery*, Vol.50, No.05, pp. 104-113. Beijing/China.

[19] Wei, L.J., Dai, F., Han, Z.S., Li, X.K., Gao, A.M. (2016). Experiment on plot wheat breeding combine harvester (小区小麦育种联合收获机试验研究) [J]. *Acta Agriculturae Zhejiangensis,* Vol.28, No.6, pp. 1082-1088. Zhejiang/China.

[20] Xiao, X.X., Li, H., Wu, C.Y., Qi, X.D., Hu, T. (2018). Motion analysis on two early-rice varieties screened in a cylindrical sieve by means of the DEM-CFD methods (基于 DEM-CFD 两种早稻品种圆筒筛清选过程的运动分析) [J]. *Journal of Mechanical Design*, Vol.35, No.10, pp. 32-37. Tianjin/China.

[21] Yuan, Z.X., Dai, F., Zhao, W.Y., Shi, R.J., Zhao, Y.M., Xin, S.L. (2023). Simulated analysis and test of air-screen cleaning device for flax based on CFD-DEM coupling (基于 CFD-DEM 的胡麻风筛式清选装置仿真分析与试验) [J]. *Transactions of the Chinese Society of Agricultural Engineering*, Vol.39, No.06, pp. 281-290. Shanxi/China.

[22] Zhu, M., Chen, H.J., Li, Y.L. (2015). Investigation and development analysis of seed industry mechanization in China (中国种业机械化现状调研与发展分析) [J]. *Transactions of the Chinese Society of Agricultural Engineering*, Vol.31, No.14, pp. 1-7. Beijing/China.